Supporting information for

Epitaxial Growth of Large-Grain-Size Ferromagnetic Monolayer CrI_3 for Valley Zeeman Splitting Enhancement

Lipeng Gong[1,#], Cheng Zhang[2,#], Anmin Nie[3,#], Changqing Lin[1], Hao Zhang[1], Chaofeng Gao[1], Meng Wang[1], Xi Zhang[4], Nannan Han[4], Huimin Su[2], Chen Lin[6], Yizheng Jin[6], Chenhui Zhang[7], Xixiang Zhang[7], Jun-Feng Dai[2,5*], Yingchun Cheng[1,4*] and Wei Huang[1,4*]

[1] Key Laboratory of Flexible Electronics & Institute of Advanced Materials, Jiangsu National Synergetic Innovation Center for Advanced Materials, Nanjing Tech University, 30 South Puzhu Road, Nanjing 211816, China

[2] Shenzhen Institute for Quantum Science and Engineering, and Department of Physics, Southern University of Science and Technology, Shenzhen 518055, China

[3] Center for High Pressure Science, State Key Lab of Metastable Materials Science and Technology, Yanshan University, Qinhuangdao 066004, China

[4] Frontiers Science Center for Flexible Electronics, Xi'an Institute of Flexible Electronics (IFE) and Xi'an Institute of Biomedical Materials & Engineering, Northwestern Polytechnical University, 127 West Youyi Road, Xi'an 710072, China

[5] Shenzhen Key Laboratory of Quantum Science and Engineering, Shenzhen 518055, China

[6] State Key Laboratory of Silicon Materials, Centre for Chemistry of High-Performance & Novel Materials, School of Materials Science and Engineering, Zhejiang University, Hangzhou 310027, China

[7] Physical Science and Engineering Division (PSE), King Abdullah University of Science and Technology (KAUST), Thuwal 23955-6900, Saudi Arabia

Methods

CVE synthesis of CrI_3. Chromium powder (-200 mesh, 99.95%, Alfa Aesar) and crystalline iodine beads (99.99+%, Alfa Aesar) were utilized as precursors. KCl (≥99.5%, Shanghai Lingfeng Chemical Reagent Co. Ltd) and KBr (≥99.0%, Shanghai Lingfeng Chemical Reagent Co. Ltd) were utilized as transport agent. The total mass of reactant mixture is 46 mg with mass ratio of Cr: I: KCl: KBr to be ca. 5: 35: 5: 1. Fluorophlogopite mica (1 × 1cm, Changchun Taiyuan Fluorophlogopite Mica Co. Ltd), amorphous quartz (1 × 1cm) and sapphire substrates were chosen as substrates. The ampoule tube was evacuated to a pressure of ~0.17 mPa and then sealed. Fig. S12 shows the size of the ampoule tube. The length, outer diameter, and thickness of the tube are 15.0, 2.0 and 0.2 cm, respectively. A neck divides the ampoule tube into growth and source zones with lengths of 5.0 and 9.5 cm, respectively. Both the outer diameter and length of the neck are 0.5 cm. The tube was loaded into a two-zone furnace. The temperatures for the source and the growth zones were raised from room temperature to 850 ℃ and 550 ℃, respectively, and then kept for 120 minutes for growth. Afterwards, both zones were naturally cooled to room temperature. The running protocol of the temperature and time for epitaxial growth is illustrated in Fig. S13.

Atomic Force Microscopy. Surface morphology and height profile of the samples were characterized by a commercial atomic force microscopy (AFM, Asylum Research Cypher S) in tapping mode settled in a glove box. The curvature radius of the tip (HQ:NSC18/Pt) is less than 30 nm and the resonant frequency of the tip is 75 kHz.

MCD measurements. The out-of-plane ferromagnetism of samples was measured using our homemade magnetic circular dichroism (MCD) system in reflection geometry. For MCD system, a He-Ne laser with a wavelength of 632.8 nm was used as an excitation. After passing through a polarizer and a photoelastic modulator (PEM), the polarization state of the incident light was modulated periodically between a linear and a circular polarized states with a frequency of 50 kHz. At last, this laser beam was focused onto sample by a 50× objective with a spot size of ~2 μm. The reflected light went through the same objective, and then was collected by a Si amplified photodetector. The corresponding MCD

signals were recorded by a lock-in amplifier. During experiments, samples were mounted on the cold finger of the closed cycle cryostat with the lowest temperature of 16 K. With the aid of a 2-dimensional spatial scanning stage, the magnetization of the whole sample can be determined with 1 μm spatial resolution. To avoid any degradation or destruction of the experimental samples during measurements, the samples were protected in N_2 environment during transfer and the excitation power was limited to 5 μW.

Raman measurements at room temperature. Raman spectra at 300 K acquired by a micro-Raman system (WITec alpha 300R) equipped with 600 grooves per millimeter gratings and a liquid-nitrogen-cooled CCD detector. A He-Ne laser (632.8nm) was focused by a microscopic objective (20×; NA = 0.4) to excite the CrI_3 sample placed in a homemade protective device at normal incidence.

Polarization-resolved micro-Raman measurements at low temperature. For the polarization-resolved Raman measurements, a 632.8 nm laser with the power of 100 μW was employed as an excitation. After passing through a polarizer and a 1/4 wave plate, the polarization of excited light was converted to a circular polarized state. The beam is then focused onto the sample using a 50× objective with a spot size of 2 μm. To distinguish the relative intensity of two circularly polarized components of Raman signals, we first converted them into two orthogonally linearly polarized lights by the same 1/4 waveplate, and separated them in space by a displacer, and focused them onto two spots on the slit of a spectrometer by a lens, and finally collected the signals using a spectrometer equipped with a thermoelectric cooled charge-coupled device (CCD). Therefore, we can record two circular components at the same time, so as to avoid experimental and system errors. A long-pass edge filter with a central wavelength of 633 nm was used to block the laser line so that the Raman signal above 100 wavenumbers can be detected. During measurements, samples were mounted on the cold finger of low temperature cryostat with the minimum temperature of 16 K.

TEM sample preparation. The scheme showing the preparation of TEM sample is presented in Fig. S2. Firstly, polymethyl methacrylate (PMMA) and poly propylene carbonate (PPC) were deposited on mica by spin-coating. Secondly, by peeling off PMMA and PPC film, the CrI_3 sample was transferred to graphene on SiO_2/Si substrate. Thirdly,

the PMMA and PPC film was removed by using acetone. Fourthly, another graphene flake was transferred on the sample to form the graphene/CrI_3/graphene heterostructure. Fifthly, the heterostructure was annealed at 500 K in high vacuum and the SiO_2/Si substrate was spin-coated with the PMMA liquid and then placed on a drier for about 2 hours at 150 ℃. Sixthly, by peeling off the film and transfer, the films were salvaged on a TEM grid and dried naturally in ambient environment for over 5 hours. Finally, the residual PMMA was removed by acetone.

STEM measurement and simulation. HAADF-STEM images of the CrI_3 were acquired by using a 24-mrad-probe convergence semi-angle, as well as a 60-mrad-inner and 200-mrad-out detector angles at 300 kV (FEI Aberration-corrected Themis Z STEM). Corresponding HAADF image simulations were conducted according to the experimental imaging parameters by using a software developed by Dr. He[1].

Calculation methods. All first-principles calculations were performed by using the projector augmented wave pseudopotentials[2] in the Vienna ab initio Simulation Package[3]. The Perdew-Burke-Ernzerhof approximation was used to describe the exchange and correlation functional[4]. The cutoff energy for the plane-wave basis was set to 450 eV and a 1 × 1 × 1 gamma-centered Monkhorst-pack k-point grids were adopted for the supercell. The convergence criteria for the electronic energy was 10^{-5} eV and the structures were relaxed until the forces on each atom is less than 0.03 eV/Å. The van der Waals interactions were included in all of our calculations within the DFT-D3 Grimme scheme[5, 6]. The calculated lattice parameters of single-layer CrI_3 (a = b = 6.90 Å, α = 90°, β = 90°, γ = 120°), fluor phlogopite mica (a = 5.33 Å, b = 9.22 Å, c = 10.21 Å, α = 90°, β = 100°, γ = 90°) are very close to the experimental values for single-layer CrI_3 (a = b = 6.87 Å, α = 90°, β = 90°, γ = 120°)[7], fluorophlogopite mica (a = 5.32 Å, b = 9.21 Å, c = 10.24 Å, α = 90°, β = 100°, γ = 90°)[8]. To model fluorophlogopite mica surface, a slab was constructed by cleaving the 4 × 2 × 1 supercell of bulk at the (001) plane, and the lattice parameters of the surface are a = 21.32 Å, b = 18.43 Å. To avoid interlayer interactions, a 20 Å vacuum was used along the z direction. To build the model of WSe_2/CrI_3 for band structure calculation, we firstly get the structure of WSe_2 and CrI_3. The in-plane lattice parameters of WSe_2 and

CrI_3 are 3.32 and 6.85 Å, respectively. A 4 × 4 supercell was used for WSe_2 and a 2 × 2 for CrI_3 to build the WSe_2/CrI_3 with lattice mismatch of 3.3%. The spin-orbit coupling effect was considered for band structure calculation.

Table S1 The coverage and area of largest flake in the optical images shown in Fig. S6.

Transport agent	**Coverage**	**Maximum area (μm^2)**
KF	4.01%	1227
KCl	9.40%	1908
KBr	10.06%	643
KCl, KBr mixture	8.20%	1474

Table S2 The energy difference of mica surface models with respect to ‘a’ model shown in Fig. S4

Surface structure	Surface energy difference (meV/Å^2)
a	0.00
b	0.06
c	0.65
d	0.84
e	0.88
f	1.60
g	1.75
h	2.47
i	3.04
j	3.12

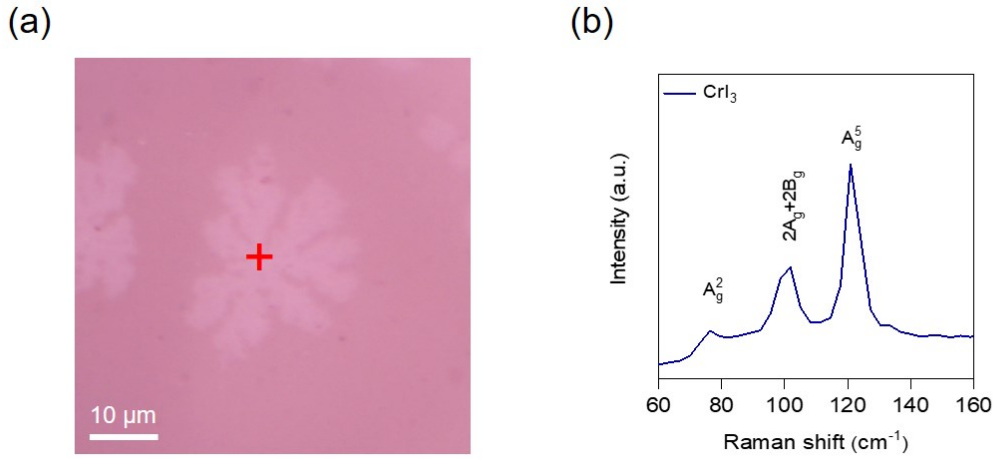

Fig. S1 (**a**) Optical image of a typical as-grown CrI_3 on mica. (**b**) Raman spectrum of the CrI_3.

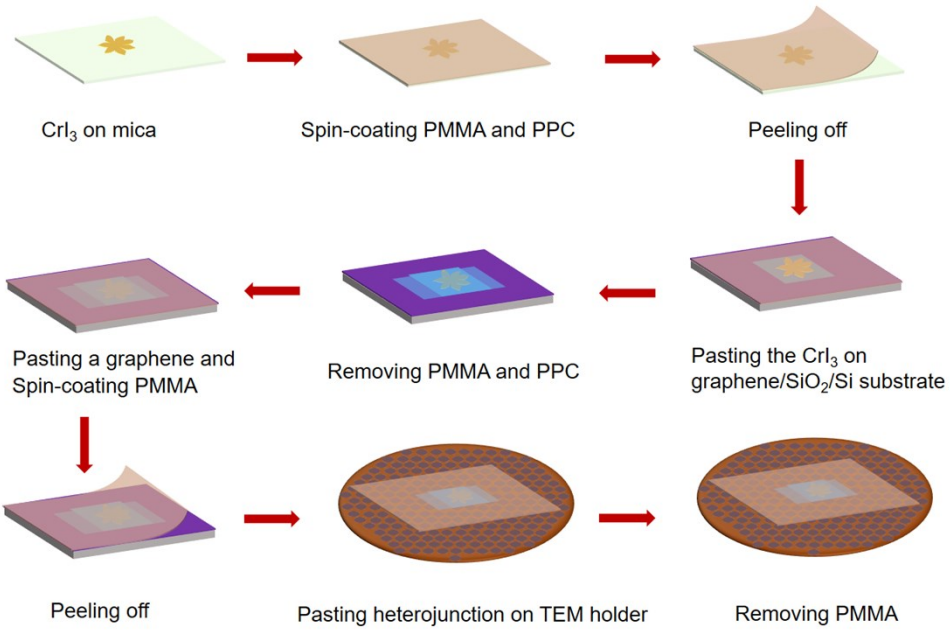

Fig. S2 Steps of preparing CrI_3 sample for STEM characterization.

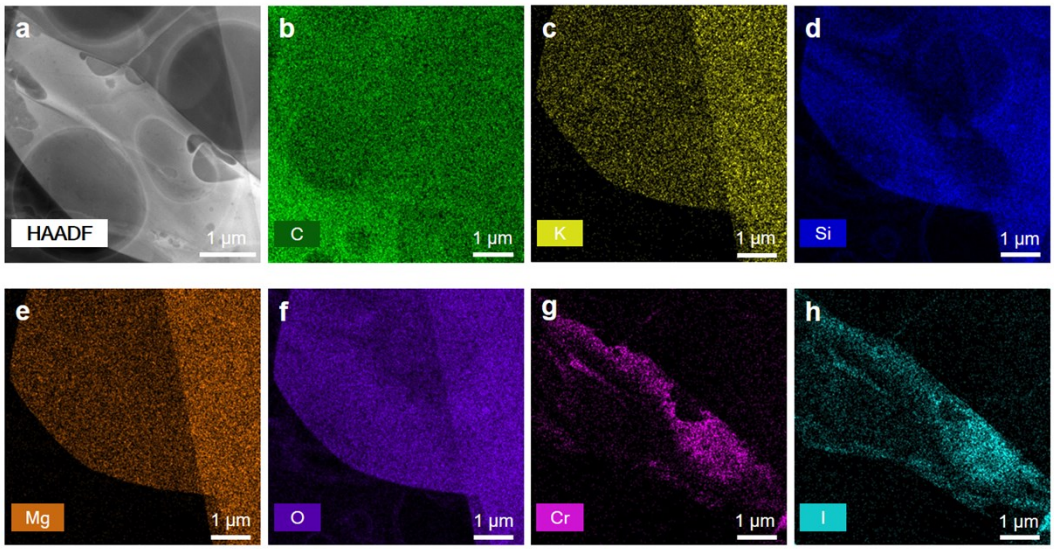

Fig. S3. (**a**) HAADF image of as-grown CrI_3. EDS mapping for (**b**) C, (**c**) K, (**d**) Si, (**e**) Mg, (**f**) O, (**g**) Cr, and (**h**) I elements. The C element mainly originated from graphene flakes, which are used to encapsulate CrI_3. The present of K, Si, Mg, and O elements is induced by residual mica adhering with CrI_3.

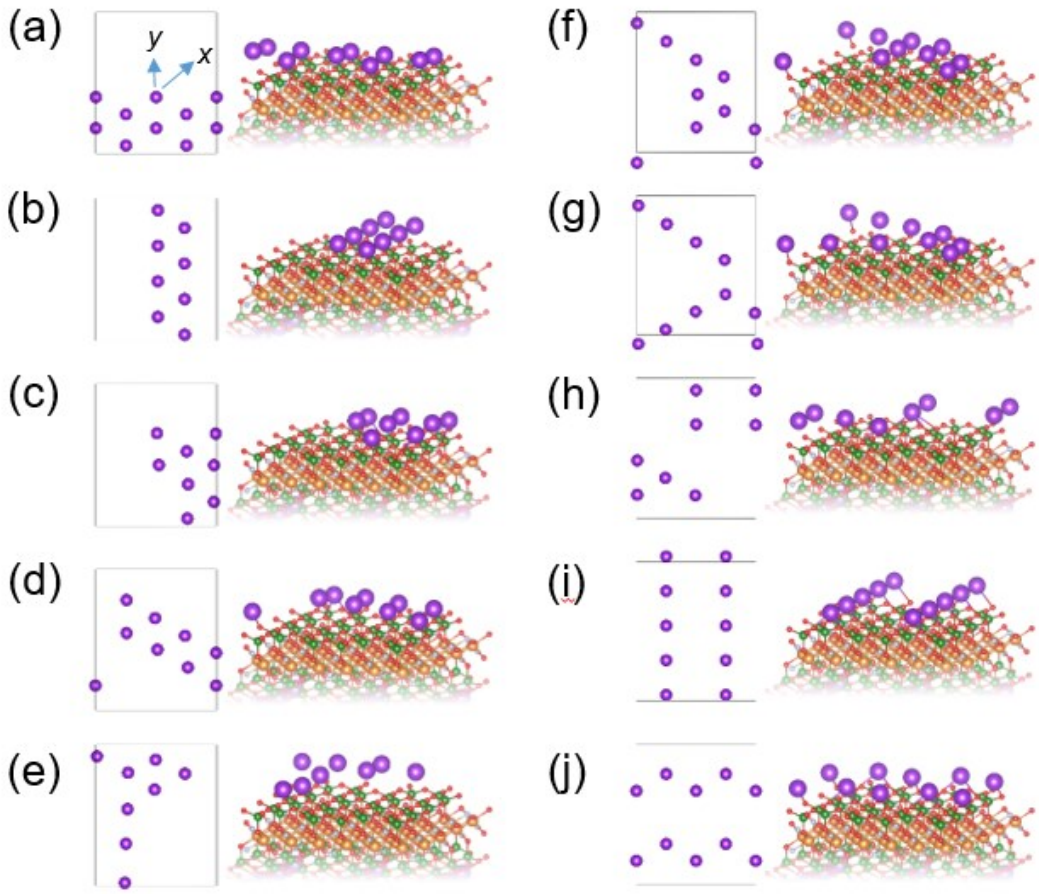

Fig. S4 (**a–j**) Top (only K ions are shown) and side views of 10 different surface structures of mica. The '*x*' and '*y*' denote the transition paths of one K ion.

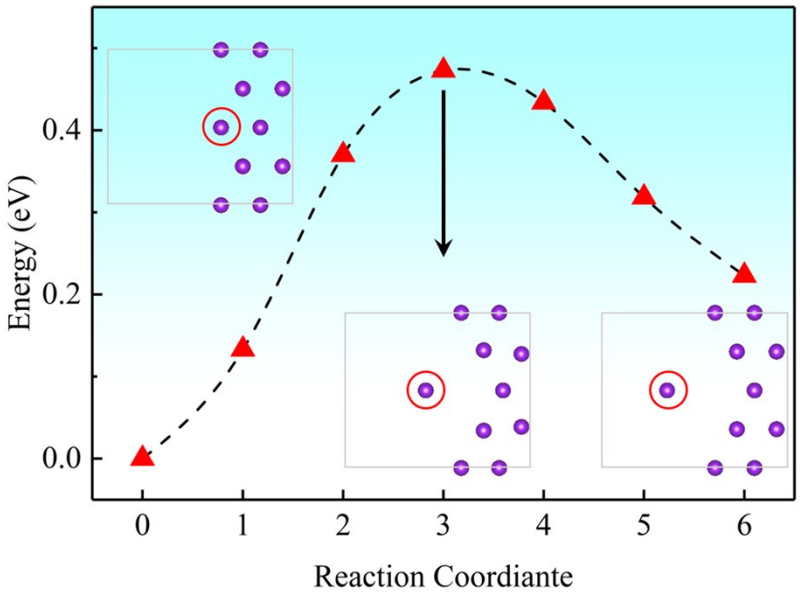

Fig. S5 Transition barrier of one K ion transporting from ground state position to a nearby position. The energy barrier is 0.48 eV.

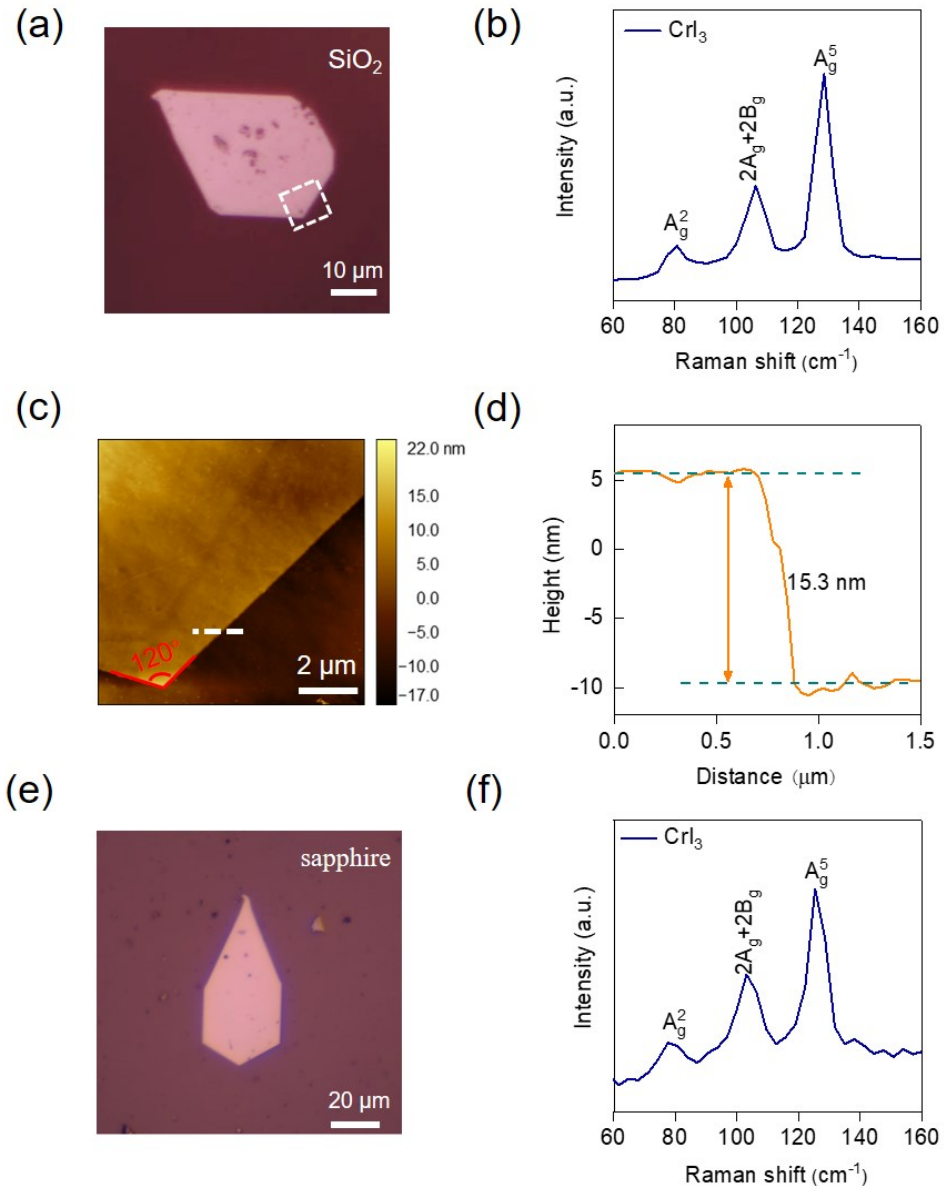

Fig. S6 Thick CrI_3 grown on quartz and sapphire substrates. (**a**) Optical image of typical CrI_3 grown on quartz substrate. (**b**) The corresponding Raman spectra of as-grown CrI_3 and quartz substrate measured at room temperature. (**c**) AFM image of the selected region (white square) in a. Scale bar is 2 μm. (**d**) Height profile along the white line in c. The height is 15.26 nm, corresponding to layer number of ~20. (**e**) Optical image of a typical CrI_3 grown on sapphire substrate. (**f**) Raman spectra of as-grown CrI_3 and sapphire substrate measured at room temperature.

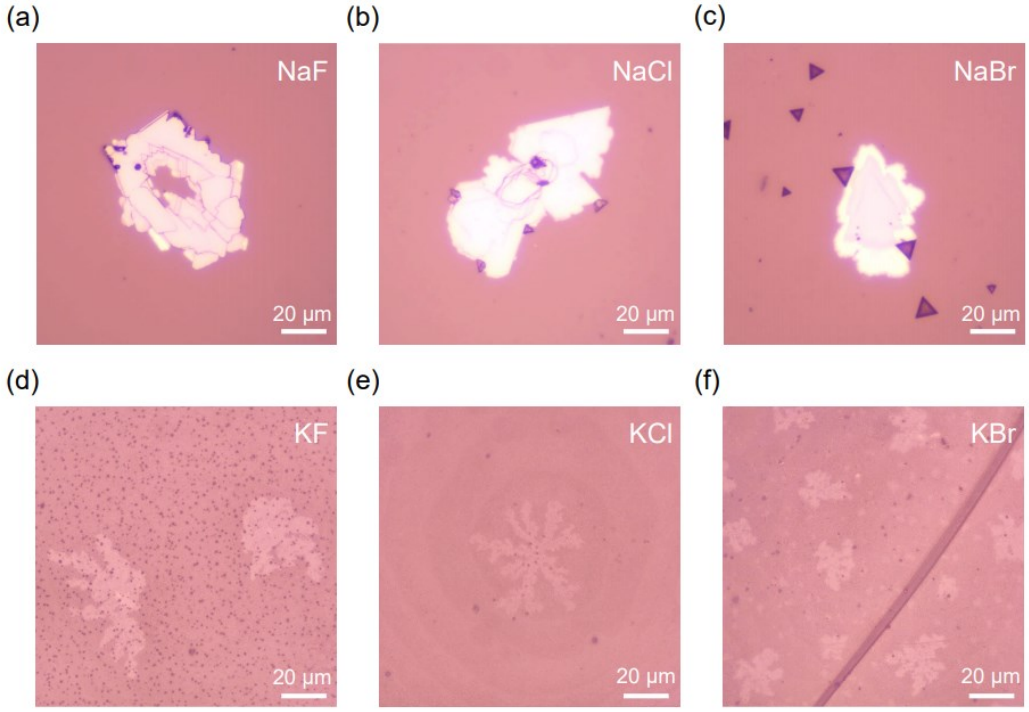

Fig. S7 Optical images of as-grown CrI_3 on mica using different transport agents. (**a**) NaF, (**b**) NaCl, (**c**) NaBr, (**d**) KF, **(e**) KCl, and (**f**) KBr**.** The black triangles in (**c**) are not CrI_3.

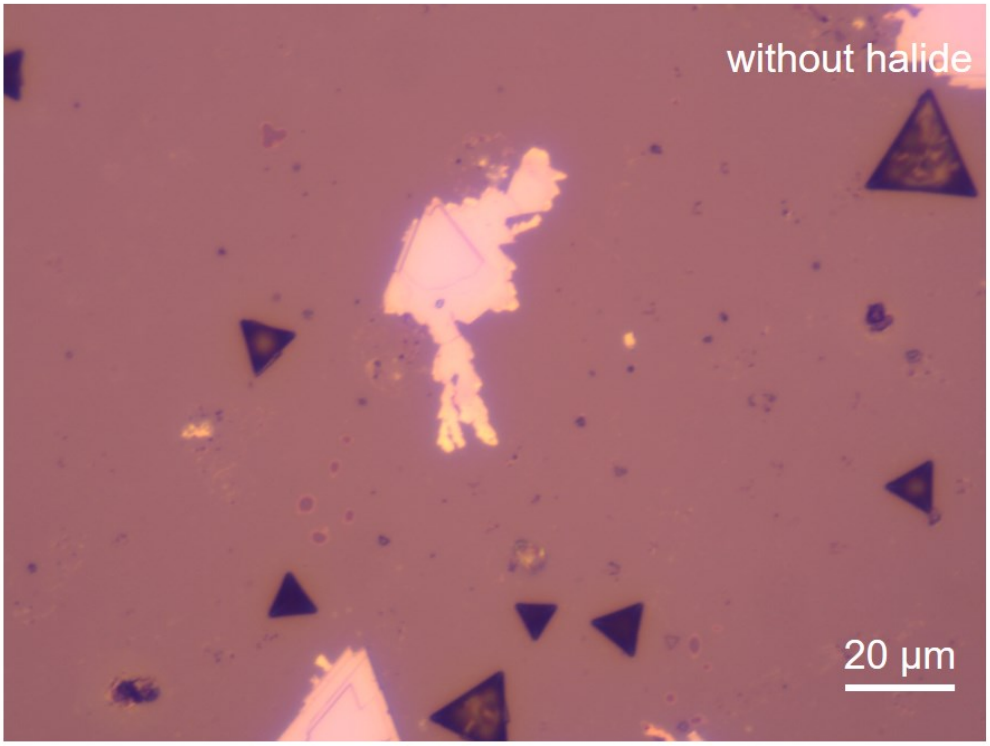

Fig. S8 Optical image of a typical sample of CrI_3 grown on mica without transport agent. The black triangles are not CrI_3 due to the absence of Raman signal.

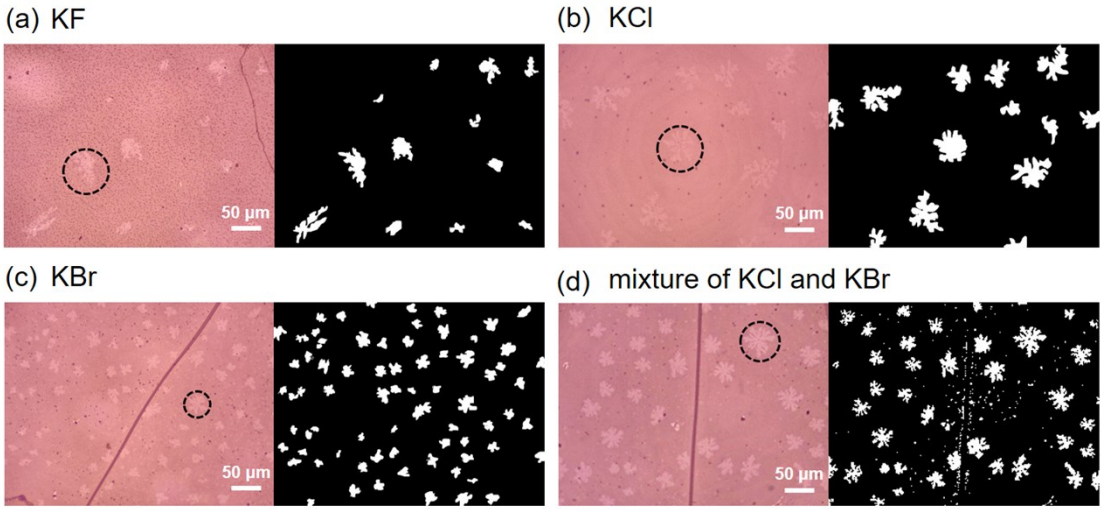

Fig. S9 Optical images together with masks of as-grown CrI_3 on mica using (**a**) KF, (**b**) KCl, (**c**) KBr, and (**d**) mixture of KCl and KBr. The masks are for identifying and calculating coverage of CrI_3 on mica. The round cycles indicate the CrI_3 monolayer with maximum area in each optical image.

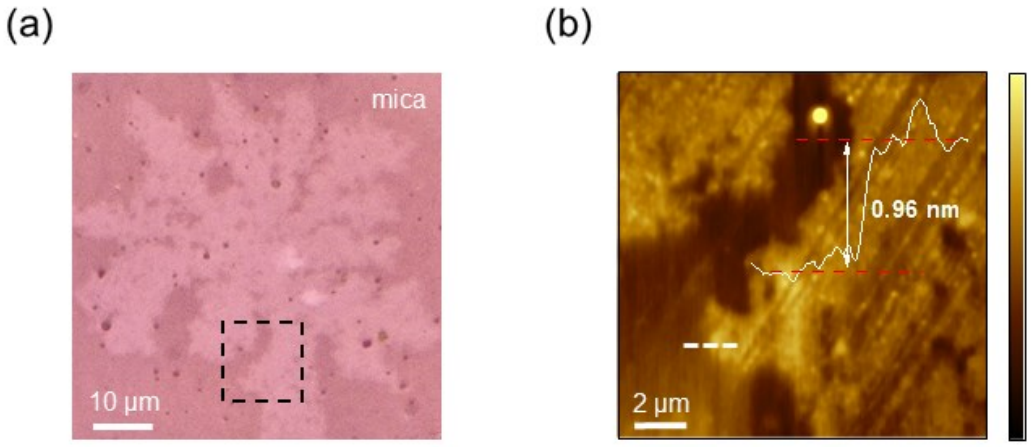

Fig. S10 (**a**) Optical image of a flowerlike monolayer CrI_3 on mica substrate, which is the same as the image shown in Fig. 4(**a**). (**b**) AFM image of the square region marked in (**a**). The height profile as indicated by the white dashed line in (**b**) shows that the layer thickness is around 0.96 nm, corresponding to a monolayer thickness.

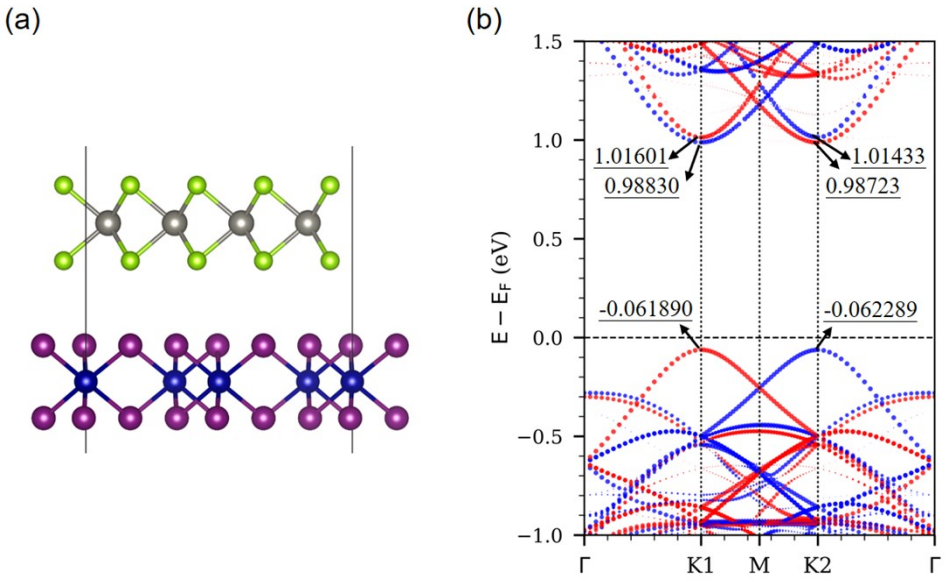

Fig. S11 (**a**) Atomic model of monolayer WSe_2/CrI_3 heterostructure. (**b**) Band structure with spin projection for orbitals from monolayer WSe_2. From the values of band edges at K1 and K2 points, it is obviously found the band edge shifts, resulting in valley Zeeman splitting.

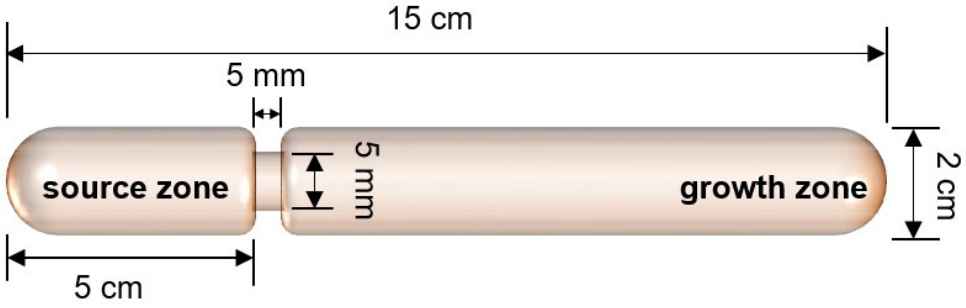

Fig. S12 The specific size of the ampoule tube for CVE growth of monolayer CrI_3.

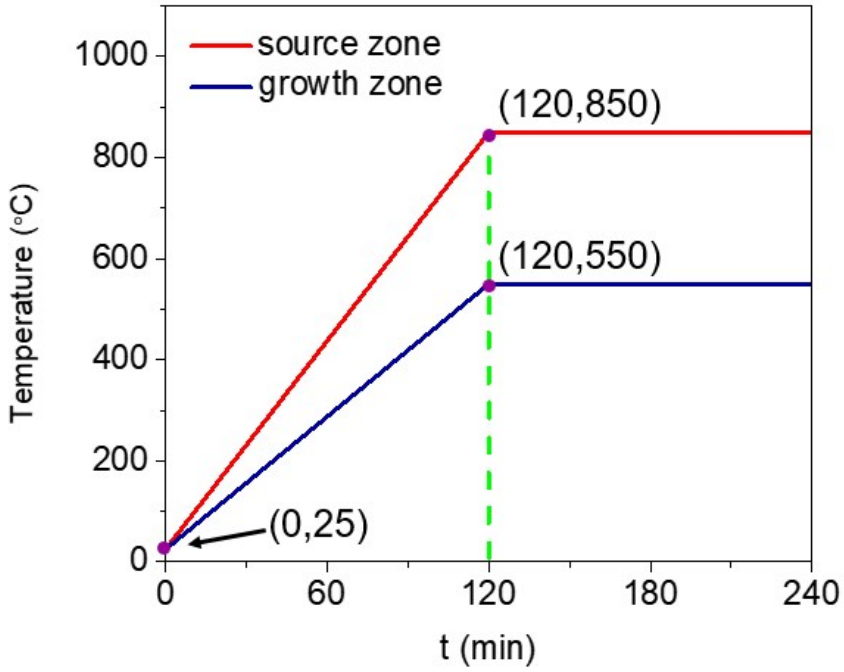

Fig. S13 Running program about temperature and time of CVE growth for monolayer CrI_3.

References

1. D. S. He, Z. Y. Li and J. Yuan, *Micron*, 2015, **74**, 47-53.
2. G. Kresse and D. Joubert, *Phys. Rev. B*, 1999, **59**, 1758-1775.
3. G. Kresse and J. Furthmuller, *Comput. Mater. Sci.*, 1996, **6**, 15-50.
4. G. Kress and D. Joubert, *Phys. Rev. Lett.*, 1999, **59**, 1758-1775.
5. S. Grimme, J. Antony, S. Ehrlich and H. Krieg, *J. Chem. Phys.*, 2010, **132**, 154104.
6. S. Grimme, S. Ehrlich and L. Goerigk, *J. Comput. Chem.*, 2011, **32**, 1456-1465.
7. B. Huang, G. Clark, E. Navarro-Moratalla, D. R. Klein, R. Cheng, K. L. Seyler, D. Zhong, E. Schmidgall, M. A. McGuire, D. H. Cobden, W. Yao, D. Xiao, P. Jarillo-Herrero and X. Xu, *Nature*, 2017, **546**, 270-273.
8. S. B. Hendricks and M. E. Jefferson, *Am. Mineral.*, 1939, **24**, 729–771.